

A Nine-Phase Permanent-Magnet Motor Drive System for an Ultrahigh-Speed Elevator

Eunsoo Jung, *Student Member, IEEE*, Hyunjae Yoo, *Member, IEEE*,
Seung-Ki Sul, *Fellow, IEEE*, Hong-Soon Choi, and Yun-Young Choi

Abstract—This paper presents a nine-phase permanent-magnet synchronous motor (PMSM) drive system based on multiple three-phase voltage source inverters. The nine-phase PMSM was developed as a traction motor for an ultrahigh-speed elevator. The mathematical model of the motor was simplified through symmetry of the system. Using the simplified model, the drive system can be controlled by the well-known $d-q$ control theory. The feasibility and validity of the drive system were experimentally demonstrated at the world's tallest elevator test tower. Moreover, an additional experiment was performed to ensure the fault-tolerance capability of the system.

Index Terms—Alternating-current (ac) motor drives, fault tolerance, high-speed elevators, industrial power system, multiphase motors.

I. INTRODUCTION

AT PRESENT, high-rise buildings are becoming more popular with advances in building technology. The advent of modern high-rise buildings has brought about the need for high-speed and/or high-capacity elevator systems to provide quick access within these buildings [1]. The definition of high speed in elevator applications varies according to the manufacturer, but the structures are similar to each other in the majority of cases. The general structure of a high-speed elevator is shown in Fig. 1. The complete system can be divided into two parts; they can be thought of separately but are dynamically coupled. The first part is a mechanical system that comprises various masses and ropes with which the parts interconnect. The second part is an electrical drive system that includes a closed-loop control system that regulates the velocity of the main sheave [2].

Manuscript received October 26, 2010; revised March 14, 2011; accepted March 22, 2011. Date of publication March 15, 2012; date of current version May 15, 2012. Paper 2010-IDC-423.R1, presented at the 2009 Energy Conversion Congress and Exposition, San Jose, CA, September 20–24, and approved for publication in the IEEE TRANSACTIONS ON INDUSTRY APPLICATIONS by the Industrial Drives Committee of the IEEE Industry Applications Society.

E. Jung is with the School of Electrical Engineering and Computer Science, Seoul National University, Seoul 151-742, Korea (e-mail: eunsoo@eepel.snu.ac.kr).

H. Yoo is with Samsung Heavy Industries Company, Ltd., Seoul, Korea (e-mail: hiyoo@eepel.snu.ac.kr).

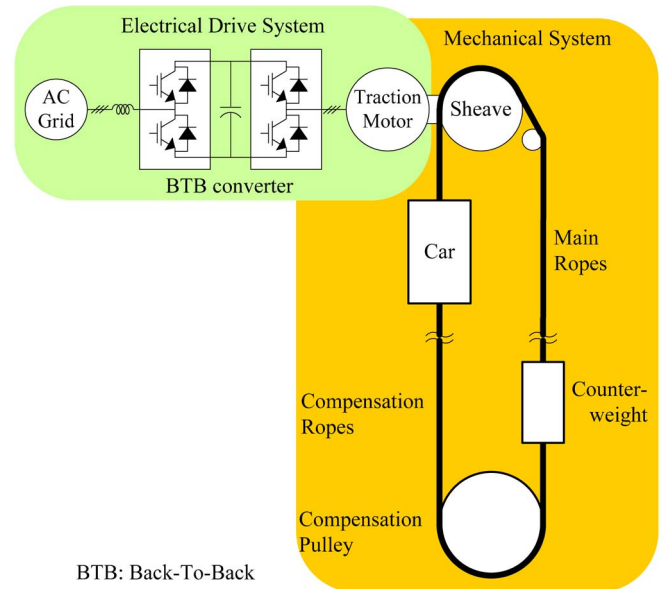
S.-K. Sul is with the School of Electrical Engineering and Computer Science, Seoul National University, Seoul 151-742, Korea (e-mail: sulsk@plaza.snu.ac.kr).

H.-S. Choi is with the School of Electrical Engineering, Kyungpook National University, Sangju 742-711, Korea (e-mail: tochs@knu.ac.kr).

Y.-Y. Choi is with the Technical R&D Center, Hyundai Elevator Company, Ltd., Icheon 467-734, Korea (e-mail: inverter@hdel.co.kr).

Color versions of one or more of the figures in this paper are available online at <http://ieeexplore.ieee.org>.

Digital Object Identifier 10.1109/TIA.2012.2190472



BTB: Back-To-Back

Fig. 1. General structure of the high-speed elevator system.

For the electrical drive system for a high-speed elevator, a combination of a voltage source back-to-back converter and a three-phase PMSM is widely used due to its regenerative capacity, compact size, and fine control performance. Because three-phase inverters have numerous advantages, they have been manufactured for elevator applications for decades. However, as the speed rating has increased, rated power of the traction system has also increased. Some high-power elevators demand a peak power rating of more than 1 MW, such as an ultrahigh-speed elevator, which moves more than 1000 m/min, and a double-deck elevator that has two cars, resembling a two-story building. Thus, a three-phase drive system may not offer a great advantage in this power range due to the limitation of the current rating of semiconductor devices.

In a high-power drive system on a low-voltage grid, multiphase motors can offset the size limitation of individual inverters. Furthermore, multiphase motors have several advantages, such as good fault-tolerance capability and a reduction in the per phase power rating [3]–[6]. These aspects have allowed dual-stator PMSMs to be adopted in state-of-the-art elevators [7]. In [7], each set of three-phase windings is separately connected to its own three-phase inverter, which employs six IGBT modules connected in parallel to increase the per phase rating of the inverter. However, when an inverter fault or a dc-link side fault occur, the relevant inverter should be detached

TABLE I
SPECIFICATION OF THE ULTRAHIGH-SPEED ELEVATOR

Rated Capacity	1600 kg (24 passengers)
Rated Speed	1080 m/min
Travel Height	540 m

from the system, after which the total power rating of the system is reduced to half of the normal operating condition.

In the event of an open fault, a control method using the other five phases could be used to minimize the total power derating of the system in [4] and [5]. However, in spite of the appropriate control, a loss of phase causes a severe torque ripple, which cannot be allowed in elevator applications. Thus, separation of the corresponding winding set from the system is greatly preferred in elevator applications.

In this paper, a nine-phase PMSM driven by triple three-phase voltage source inverters (VSIs) is introduced for an ultrahigh-speed elevator. The mathematical model of the nine-phase motor was divided into three independent three-phase motor models through symmetry between the winding sets and the current controllers. With this simple model, three conventional synchronous-frame proportional and integral (PI) current controllers can be easily applied to the nine-phase motor without the need for a complex multiphase machine theory. Experiments with the nine-phase motor, which is a traction machine of an ultrahigh-speed elevator, were performed to evaluate the validity of the drive system.

II. ELECTRICAL DRIVE SYSTEM DESIGN

The proposed electric drive system for the ultrahigh-speed elevator consists of a nine-phase PMSM, three grid-side converters with interface inductors, three motor-side inverters with dv/dt suppression filters, and a DSP-FPGA controller. In this chapter, the system specification and detail of the electric drive system are explained.

A. System Specification

The specification of the ultrahigh-speed elevator is shown in Table I. The rated speed of the car is 1080 m/min, at which speed it takes 45 s to move up 540 m. The rated capacity for passengers is 1600 kg, which is equivalent to 24 passengers. If this elevator is installed in a commercial building, it will be the fastest elevator in the world.

B. Traction Motor

A computer simulation based on a simple mechanical model was performed to calculate the desired capacity of the traction motor. The passenger capacity is 1600 kg, but other mechanical parts to support this capacity are much heavier. The total mass was assumed to be 40 000 kg considering the weight of the mechanical system such as the car, the counterweight, the main ropes, and the compensation ropes, as shown in Fig. 1. Any unbalanced condition between the car and the counterweight is considered to be 800 kg, which is the maximum value.

The simulation result of the elevator operation is shown in Fig. 2. The top figure shows the speed reference profile of

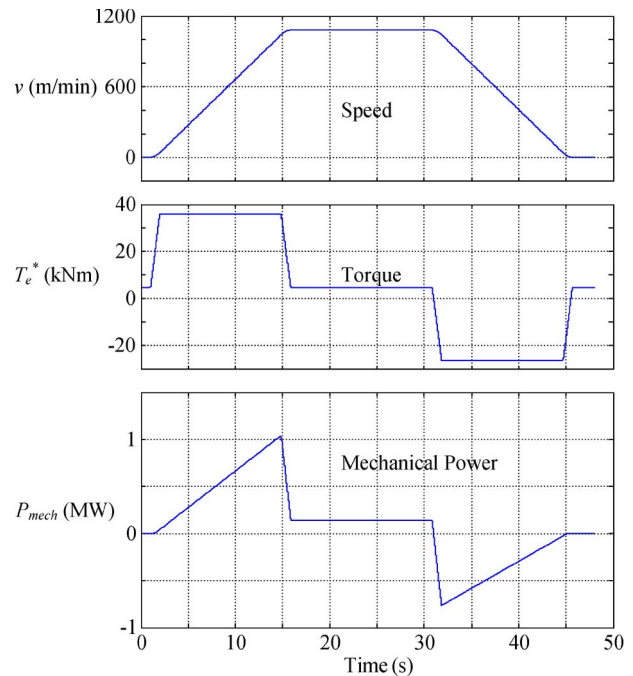


Fig. 2. Simulation result for ultrahigh-speed operation under a maximum load condition.

the car, which moves up for 540 m. The acceleration value is 1.3 m/s^2 in the ramp section. This is the maximum acceleration value at which passengers do not feel uncomfortable. The necessary torque of the motor is 36 kNm at this time. According to the simulation results, the traction motor requires maximum mechanical power of more than 1 MW to meet the specifications in Table I. These results are based on an ideal operating condition. Reflecting the loss of the motor, the total power rating should be increased further. Assuming that the total efficiency of the entire mechanical system is 0.9 including the design margin, the maximum output power of the motor should be more than 1.1 MW.

Medium voltages are generally not available in commercial buildings where elevators are installed. Elevator drive systems are thus usually connected to a low-voltage grid. Considering that the grid voltage is 380 V and the dc-link voltage is 680 V, the terminal voltages of the motor should be similar to the grid voltage at the rated speed. The power factor of the motor is approximately 0.95 at the peak power of 1.1 MW. The peak output current of the VSI therefore easily exceeds 2500 A, in the case of a three-phase traction motor. Because such a high-current 1200-V IGBT device module does not exist, a group of devices has to be connected in parallel to satisfy this high current level.

In this paper, a nine-phase PMSM was applied for the ultrahigh-speed elevator to reduce the current rating of each phase. Assuming that the back electromagnetic force (EMF) of the nine-phase motor is identical to that of the three-phase case, the rated current can be reduced to one-third of that of the three-phase motor. This permits the use of a single power device for each inverter switch instead of a group of devices connected in parallel. Moreover, because multiphase motors have lower torque ripple characteristics and open-phase fault tolerance, it becomes possible to improve the ride comfort and safety of the passengers with higher reliability at the system level.

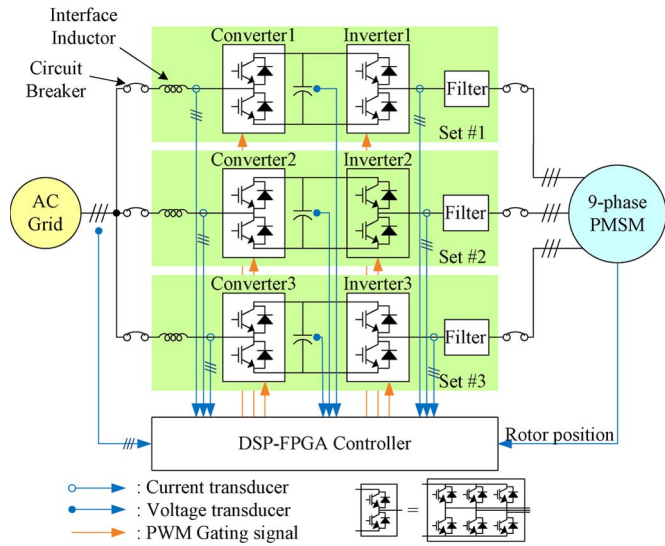


Fig. 3. Developed electrical drive system for an ultrahigh-speed elevator.

C. Motor Drive System–Pulsewidth Modulation (PWM) Inverters and Converters

Traction motors have to generate high torque regardless of the operating speed for elevator applications. Thus, the power conversion unit should offer rated current at any operation speed. Additionally, the elevator driven by an electrical motor demands a bidirectional power flow control to handle motoring and generating power, which repeatedly arise during acceleration and deceleration operations. Therefore, a voltage source back-to-back converter is widely used in high-speed elevators due to its regenerative capability. It is also possible in this way for the power factor at the grid side to be maintained at unity and for the dc-link voltage to be kept at a desired value [2].

To drive the nine-phase PMSM, three sets of back-to-back converters developed for high-speed elevators of the 600 m/min class were adopted. The parallel operation of three sets of the converters can bring a cost advantage due to mass production. The grid-side converters are connected to each other at the utility grid by interface inductors, as shown in Fig. 3. To improve the level of system reliability, the dc-links are separated from each other because a common dc-link structure is not capable of supporting severe faults in the dc-bus [4]. Each back-to-back converter operates independently and consists of six IGBTs, whose rating is 1200 V and 1200 A at 80 °C. The rated power of each back-to-back converter is 450 kW; thus, the overall system can deliver 1.35 MW in total.

Each utility side converter includes interface inductors to regulate the current to the utility grid. The size of these interface inductors is determined by the limitation of the magnitude of the switching current ripple to the utility side. To reduce this current ripple, the carriers of three PWM converters are interleaved with each other by one-third of the switching period. This reduces the magnitude of the current ripple significantly.

There are circuit breakers for the input terminals of the converters and the output terminals of the inverters to increase the reliability of system. When a fault occurs, the circuit breakers of the corresponding set are opened, and the faulty set can then be separated from the entire system, and the remaining

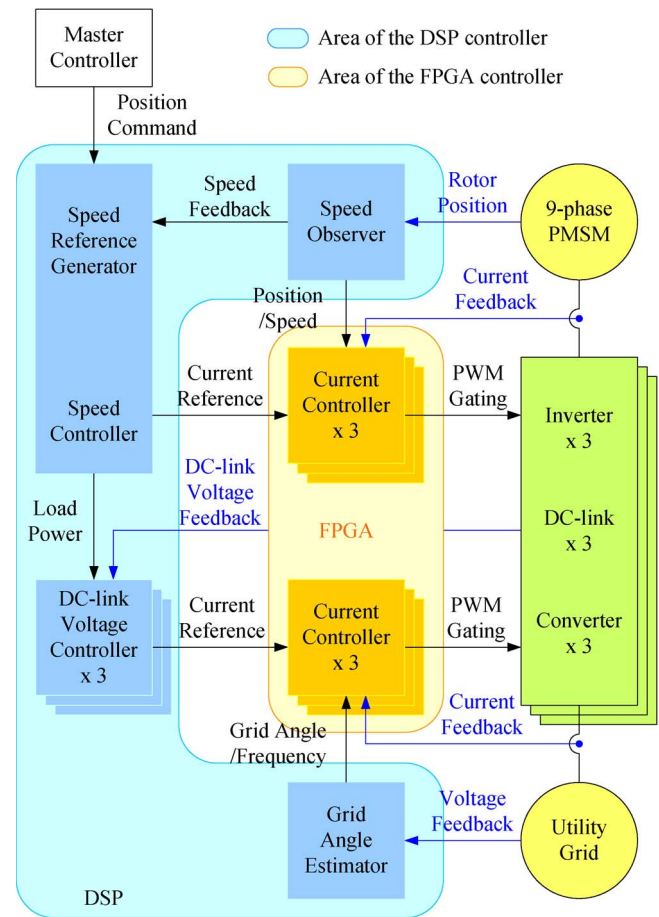


Fig. 4. Configuration of the control board.

sets can still perform their normal operations. In the case of the separation of one set, the total power rating becomes approximately two third of the unfaulted system power rating.

To improve the reliability of the system against a high dv/dt condition, a filter inductor and an RC network were included between the inverter and the motor. The filter inductor and the RC network suppress spike voltages at the motor terminals and prevent the motor from insulation failure.

D. Control Board

The control board consists of two controllers: The first is a digital signal processor (DSP) controller, and the second is a field-programmable gate array (FPGA) controller to release the load of the DSP. The detail configuration of the control board is shown in Fig. 4. The main objectives of the DSP controller are the tracking of the motor speed reference and the regulation of the three dc-link voltages. The FPGA controller takes charge all of the current control to assist the DSP controller.

A master controller such as an elevator group controller gives a position reference to the DSP controller. The speed reference generator inside of the DSP controller then creates speed and acceleration references that have a very smooth waveform so as not to excite the resonance of the mechanical system. The speed controller calculates the torque reference to minimize the speed and acceleration error. Other tasks of the DSP are the estimation of the rotor speed from the rotor position and detection of the

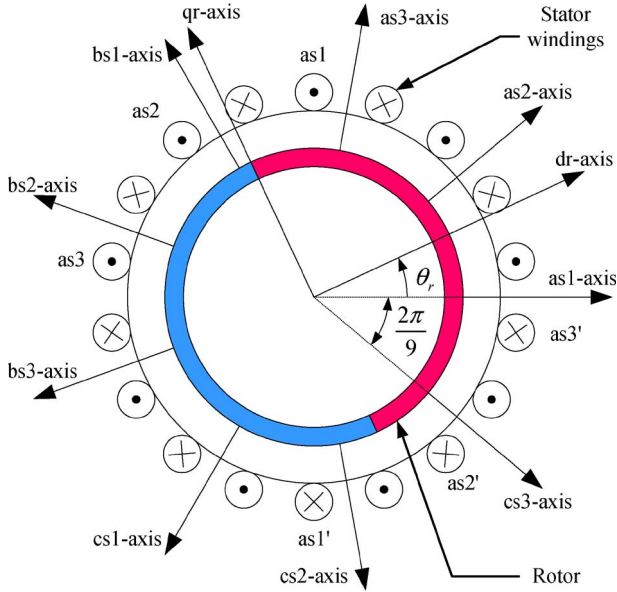


Fig. 5. Simplified structure of the nine-phase PMSM.

grid angle and frequency from the grid voltages. At the end of the calculation, the DSP gives the current references, angles, and angular velocities of the motor and the grid to the FPGA current controller.

The FPGA controller has six three-phase current controllers to regulate all of the inverter and converter output currents: Three of them are for the nine-phase motor drive, and the other three are for the grid current control. The FPGA has 36 channels of carrier-based PWM signal generators for gating, and all of the carriers can be phase-shifted with respect to the reference carrier. The FPGA also detects hardware faults to protect the system.

III. MODELING AND CONTROL

To control the drive system, a mathematical model of the nine-phase PMSM should be initially derived. Following this, the control strategy of the system is proposed.

A. Structure of the Nine-Phase PMSM

The structure of a nine-phase motor was simplified for easy understanding. The simplified motor has two rotor poles and nine stator windings, as shown in Fig. 5. The notation in Fig. 5 represents the phase name and the three-phase set number. For example, $b2$ stands for the b -phase of the second three-phase set. Each stator winding is expressed as one coil per phase, but in a real machine, it is a bunch of distributed windings to obtain a sinusoidal back EMF. The stator windings are directed along the magnetic axis of the respective phase. For example, the current that flows along the $a1 - a1'$ winding generates the magnetic flux along the $a1$ -axis.

Three windings separated by $2\pi/3$ rad in terms of the electrical angle as regards each other are connected in a wye to constitute one three-phase winding set. That is, the nine-phase motor can be considered as a triple three-phase set with three isolated neutral points. The adjacent three-phase sets are

spatially displaced by $2\pi/9$ rad, which is the angular spacing between multiple winding sets to minimize the pulsating torque of the nine-phase machines [8]–[10].

An asymmetric winding arrangement with the $\pi/9$ spacing was used in some earlier studies [9]–[11]. However, an asymmetric arrangement is equivalent to a symmetric arrangement with the $2\pi/9$ spacing [9]. By rotating the third three-phase set by 180° , asymmetric winding can be achieved. Hereafter, the symmetric winding arrangement will be used to focus on the symmetry of the system.

B. Mathematical Model of the Nine-Phase PMSM

Many papers have been published that describe a model of multiple three-phase stator sets, particularly for dual three-phase motors [8]–[14]. There are two main approaches to model a dual three-phase motor: The first is through vector space decomposition (VSD), and the second is through an extension of the three-phase model.

According to the VSD theory, the 6-D current space can be divided into the $\alpha - \beta$ subspace and other subspaces related to zero sequences and high-order harmonics. The VSD approach is useful in dual three-phase machine control because the resultant model is nearly identical to the model of a three-phase machine. Thus, the $\alpha - \beta$ currents can be easily controlled by a synchronous-frame current controller. These aspects can be extended to triple three-phase motors. However, with this model, it is hard to apply the synchronous-frame current controller to the other harmonic components.

Another modeling approach is the multiple three-phase model. The nine-phase current can be expressed as a combination of three three-phase sets, which are coupled to each other. Thus, synchronous-frame current controllers can be applied to each three-phase model with some decoupling schemes. The stator voltage equations of the nine-phase PMSM can be obtained from the multiple three-phase motor model expressed in the arbitrary $d - q$ reference frame [8]. Thus, the stator voltages in complex vector notation can be expressed as follows:

$$\begin{bmatrix} \bar{v}_{dq s1}^r \\ \bar{v}_{dq s2}^r \\ \bar{v}_{dq s3}^r \end{bmatrix} = R_s \begin{bmatrix} \bar{i}_{dq s1}^r \\ \bar{i}_{dq s2}^r \\ \bar{i}_{dq s3}^r \end{bmatrix} + p \begin{bmatrix} \bar{\lambda}_{dq s1}^r \\ \bar{\lambda}_{dq s2}^r \\ \bar{\lambda}_{dq s3}^r \end{bmatrix} + j\omega_r \begin{bmatrix} \bar{\lambda}_{dq s1}^r \\ \bar{\lambda}_{dq s2}^r \\ \bar{\lambda}_{dq s3}^r \end{bmatrix}. \quad (1)$$

The complex variables in the $d - q$ rotor reference frame are defined as $\bar{x}_{dqsk}^r = x_{dsk}^r + jx_{qsk}^r$, where the subscript k denotes the winding set number. In addition, R_s is the stator resistance, and ω_r is the electrical angular velocity of the rotor. The flux linkage equations for the k th three-phase set can be written as

$$\begin{aligned} \lambda_{dsk}^r &= L_{ls} i_{dsk}^r + \frac{3}{2} L_{ms} \sum_{j=1}^3 i_{dsj}^r + \lambda_f \\ \lambda_{qsk}^r &= L_{ls} i_{qsk}^r + \frac{3}{2} L_{ms} \sum_{j=1}^3 i_{qsj}^r. \end{aligned} \quad (2)$$

Here, λ_{dsk}^r and λ_{qsk}^r denote d -axis and q -axis flux linkage of the k th three-phase set. L_{ls} and L_{ms} represent the leakage inductance and mutual inductance, respectively, and λ_f is the

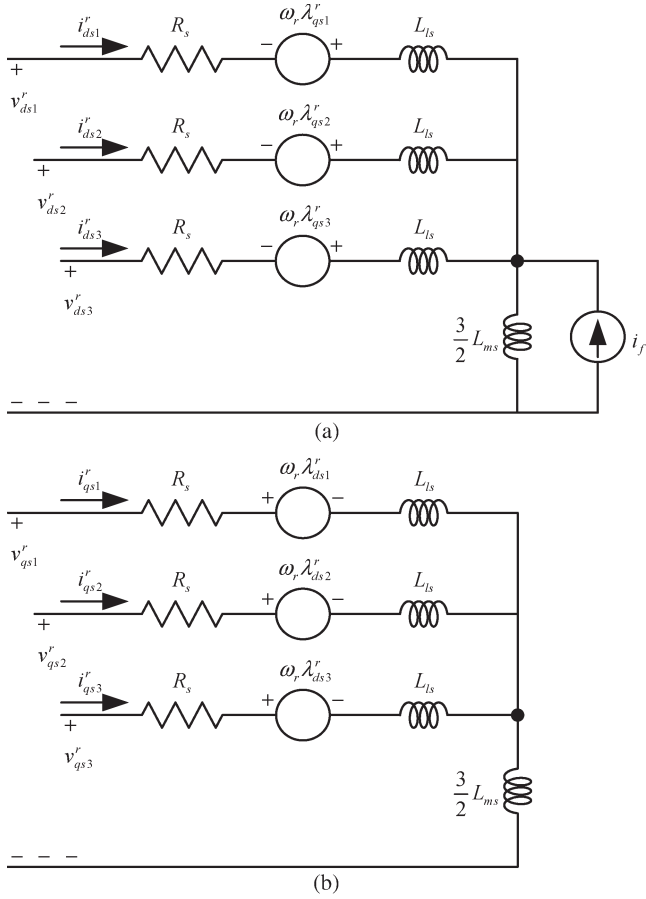


Fig. 6. Equivalent circuits of a nine-phase PMSM in the d - q rotor reference frame. (a) d -axis circuit. (b) q -axis circuit.

flux linkage between the stator windings and the permanent magnet. The equivalent circuits of the nine-phase PMSM, in the d - q rotor reference frame, are depicted in Fig. 6. The current source i_f is the field current, equivalent to the flux linkage, due to the permanent magnet.

In a surface-mounted PMSM, the current that contributes to the torque generation is only the rotor reference q -axis component because the back EMF is induced by the permanent magnet existing in the rotor reference q -axis and because there is no saliency. Thus, the torque generated by the k th set can be described as

$$T_{ek} = \frac{3P}{2} \lambda_f i_{qsk}^r. \quad (3)$$

In this equation, P represents the number of poles. There are three independent winding sets; thus, the total torque is the sum of the torque generated by each sets. As a consequence, the total torque generated by the nine-phase motor can be expressed as

$$T_e = \frac{3P}{2} \lambda_f (i_{qs1}^r + i_{qs2}^r + i_{qs3}^r). \quad (4)$$

C. Motor Control Strategy

In [15]–[17], two sets of d - q synchronous-frame current controllers were used for the dual three-phase motor drive. To decouple the magnetic interconnection between the two

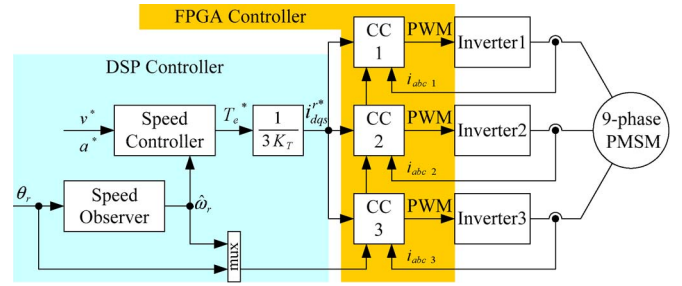


Fig. 7. Control scheme for the proposed nine-phase motor drive system.

stator windings, a complex decoupler was designed based on a mathematical model. In this paper, the complex decoupler for the current controller is simplified through symmetry of the winding sets and current controllers.

The triple three-phase motor has six independent currents because the zero sequence of each set is zero. Thus, six current controllers are needed to regulate all of independent current states to desired values. The control scheme for the nine-phase PMSM drive system is shown in Fig. 7. It is a cascade structure made up of one speed controller and three sets of d - q synchronous-frame current controllers. The speed controller receives the speed and acceleration reference and generates the torque reference T_e^* , and the torque reference is converted to the current reference according to (4). Under normal operation, to minimize copper loss in the motor, the current reference of each inverter is maintained at the same value

$$\begin{aligned} i_{qs1}^{r*} &= i_{qs2}^{r*} = i_{qs3}^{r*} = \frac{T_e^*}{3 \left(\frac{3P}{2} \lambda_f \right)} \\ i_{ds1}^{r*} &= i_{ds2}^{r*} = i_{ds3}^{r*} = 0. \end{aligned} \quad (5)$$

The output voltages of k th-set synchronous-frame PI current controllers with back EMF compensation can be written as

$$\begin{aligned} v_{dqsk}^{r*} &= K_p (i_{dqsk}^{r*} - i_{dqsk}^r) \\ &\quad + K_i \int (i_{dqsk}^{r*} - i_{dqsk}^r) dt + v_{dqsk_ff}^r - R_v i_{dqsk}^r \\ v_{dsk_ff}^r &= -\omega_r \lambda_{qsk}^r \\ v_{qsk_ff}^r &= \omega_r \lambda_{dsk}^r. \end{aligned} \quad (6)$$

Here, K_p and K_i denote the PI gains, respectively. R_v is the active resistance that suppresses the dynamic responses due to parameter errors and voltage disturbance [18].

Three sets of d - q current controllers have the same structure with the same current reference. The structure of the winding sets is symmetric. Thus, although the linkage flux term is a function of three independent d - q current sets, the current responses of the three-phase sets are identical to each other, i.e., $i_{dq1}^r = i_{dq2}^r = i_{dq3}^r$. Therefore, the flux linkage equation (2) can be simplified as

$$\begin{aligned} \lambda_{dsk}^r &= \left(L_{ls} + 3 \frac{3}{2} L_{ms} \right) i_{dsk}^r + \lambda_f \\ \lambda_{qsk}^r &= \left(L_{ls} + 3 \frac{3}{2} L_{ms} \right) i_{qsk}^r. \end{aligned} \quad (7)$$

Replacing $L_{ls} + (9/2)L_{ms}$ by L_s , which is termed as the synchronous inductance, the voltage equation of each set is

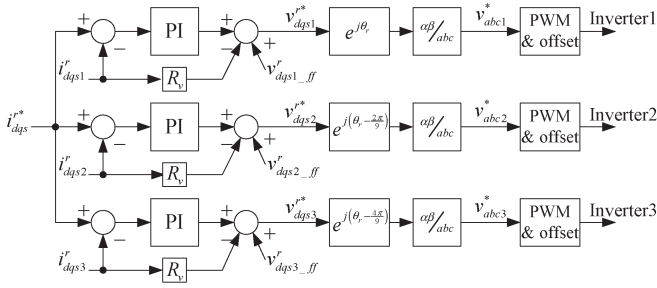


Fig. 8. Block diagram of the current controllers.

decoupled from each other and becomes identical to that of a general three-phase PMSM, as described in [19]

$$\begin{aligned} \lambda_{dsk}^r &= L_s i_{dsk}^r + \lambda_f \\ \lambda_{qsk}^r &= L_s i_{qsk}^r. \end{aligned} \quad (8)$$

A block diagram of the current controllers is shown in Fig. 8. Using the simplified motor model, the nine-phase motor can be driven by three $d-q$ synchronous-frame controllers without any complex multiphase machine control theories. Moreover, because the output of the current controller is the phase voltage of each inverter set, a three-phase PWM strategy is also directly applicable. Thus, the PWM strategy based on the offset voltage with a triangular carrier wave, as introduced in [20], was adopted for each inverter voltage synthesis.

Imbalance among inverter systems or asymmetry among the winding sets can cause an unbalanced result in the current transient response. However, a large amount of imbalance is not likely to exist under normal operation, although small amounts in addition to low asymmetry due to manufacturing tolerance and control imbalance may arise as a type of disturbance. The disturbances are sufficiently rejected by each feedback controller with active resistance. Thus, any imbalance or asymmetry is not an issue when they are small enough. The experimental results in the next section reveal reasonably satisfactory performance.

IV. EXPERIMENTAL RESULTS

To evaluate the validity of the proposed system, the nine-phase PMSM and its drive system were developed, and an ultrahigh-speed elevator system was installed in the world’s tallest elevator test tower. The developed nine-phase PMSM and the test tower are shown in Fig. 9. The parameters of the motor are listed in Table II.

Before the installation of the elevator, experiments were done under various load conditions on the ground. To confirm the back EMF of the motor, the entire inverter gating signal was turned off while operating it under a constant speed operation. The line-to-line voltage waveforms of the three sets during natural deceleration from 140 r/min are shown in Fig. 10. The bottom figure shows the magnified waveform of the red block in the top figure. The line-to-line RMS of the fundamental component is 370 V, and its fifth-order harmonics is 3% of the fundamental component based on the FFT results.

The steady-state waveform of three a -phase output currents is shown in Fig. 11, when the synchronous frequency is 60 Hz

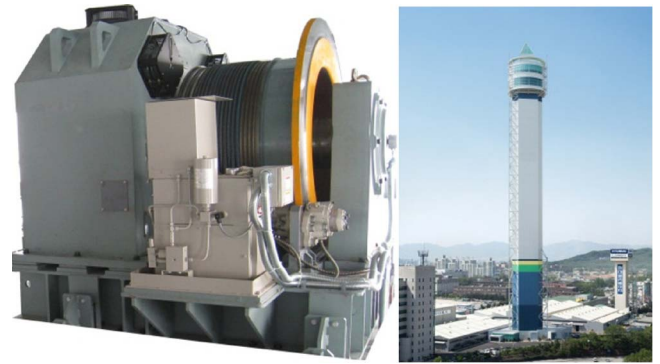


Fig. 9. (Left) Nine-phase PMSM and (right) the elevator test tower.

TABLE II
PARAMETERS OF THE DEVELOPED NINE-PHASE PMSM

Maximum Power	1.1 MW
Maximum Torque	40 kNm
Rated Speed of the Sheave	1,080 m/min
Phase Resistance	20 mΩ
Phase Inductance	0.28 mH

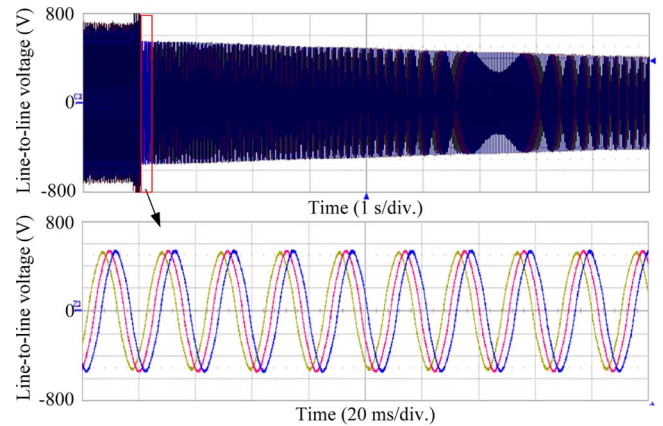


Fig. 10. Line-to-line voltage of (top) the nine-phase motor and (bottom) the magnified waveform of the top figure.

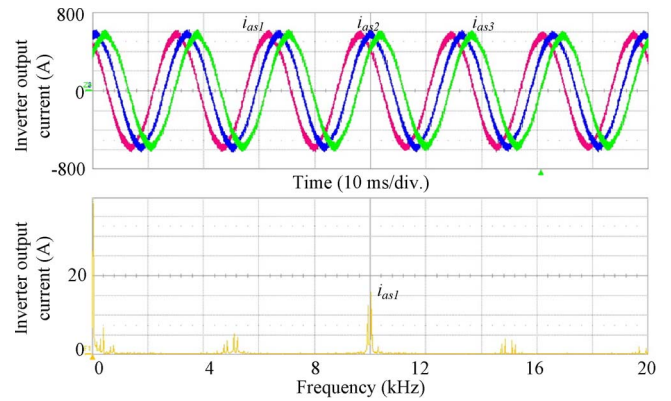


Fig. 11. Inverter output current waveform and its FFT result when the synchronous frequency is 60 Hz.

and when the switching frequency is 5 kHz. The phase currents of each inverter are well balanced and phase-shifted by $2\pi/9$ rad, and the magnitude of all harmonic currents, except twice the switching frequency, is less than 1% of the fundamental component, as shown in the FFT result.

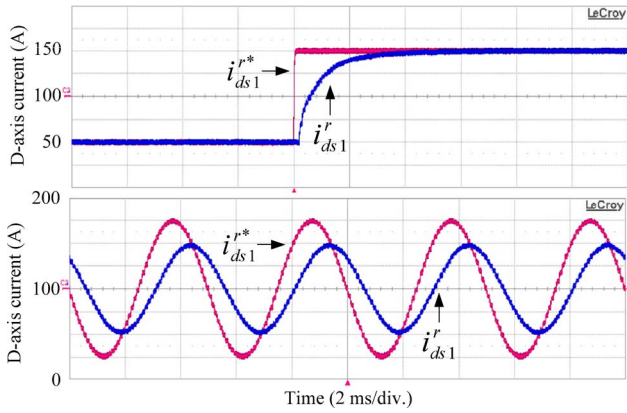


Fig. 12. Current control performance of the nine-phase motor at a constant speed of 4 r/min, with (top) the step change of the d -axis current reference and (bottom) the sinusoidal change of the d -axis current reference.

While the q -axis current controller generates torque for the speed control, the d -axis current references of the three sets were changed to determine the dynamic performance of the current controller. The current response of the Inverter 1 set against the step and sinusoidal reference changes are shown in Fig. 12. The cutoff frequency of the closed-loop current controllers was set to 1200 rad/s based on the derived model, which indicates $K_p = L_s \omega_{cutoff}$ and $K_i = (R_s + R_v) \omega_{cutoff}$. The speed was set to a constant speed of 4 r/min. In the top figure, the d -axis reference is instantaneously changed from 50 to 150 A. The rising time of the current feedback is about 1.8 ms. In the bottom figure, the d -axis reference has a sinusoidal waveform whose frequency is 200 Hz. The phase delay between the reference and feedback is about 45° . These two results confirm that the bandwidth of the controller is identical to that of the designed value. Thus, the feasibility of the simplified motor model with three d - q synchronous-frame controllers is confirmed by the experiment results shown in Figs. 11 and 12.

To validate the functionality of the nine-phase motor and its drive system, a load test was performed on the ground. The nine-phase motor was installed and connected to a load motor and inertia by the mechanical gear. The load motor emulates the weight unbalance. The inertia is equivalent to that of an elevator whose stroke is 540 m. The load test result under the same condition as the ultrahigh-speed elevator operation is shown Fig. 13. The figures from top to bottom represent the equivalent car position, the speed reference, the speed feedback, the torque reference, the Converter 1 a -phase current and the Inverter1 a -phase current.

The elevator operation can be divided into three sections: the first is for acceleration, the second is the constant speed section, and the last is the deceleration section (see Fig. 13). During the acceleration period, which takes 15 s from 0 to 1080 m/min, the nine-phase motor generates near maximum torque to accelerate the inertia up to the rated speed. As the car speed is increased, the motor output power is also increased. Thus, at the end of the acceleration, the motor output power, which is a product of the speed and torque, becomes 1 MW. The ringing torque component at the beginning of the acceleration arises, owing to the gear coupling dynamics, although this does not exist in an

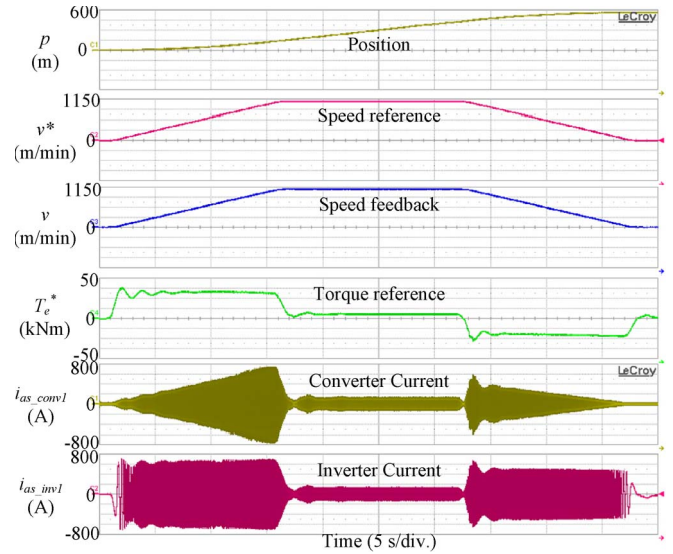


Fig. 13. Load test on the ground under the same condition as the *ultra* high-speed elevator operation.

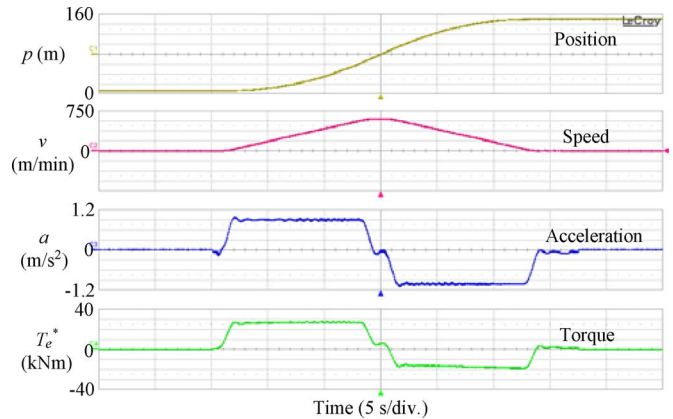


Fig. 14. Operation of the elevator from the first to the 47th floor in the test tower.

actual elevator system. After the acceleration, the speed is kept constant with a synchronous frequency of 100 Hz withstanding the load torque, which is mainly due to the weight imbalance between the car and the counterweight. This unbalanced load was set as the maximum and was emulated by the load motor. In the deceleration section, the converters transfer regenerative power from the kinetic energy to the grid. During this section, because the load torque assists with the deceleration, the motor torque is less than that during the acceleration section.

Fig. 14 shows the operation result of the ultrahigh-speed elevator from the first to the 47th floor in the test tower when the car is full. The test tower is the world's tallest elevator test tower but its stroke is 156 m, which is not enough to accelerate the car up to 1080 m/min. Thus, the nine-phase motor and its drive system were tested as a 600 m/min double-deck elevator to match the load condition to that of a 1080 m/min class elevator. In this case, the maximum acceleration was set as 0.8 m/s^2 . For the first 10 s, idle states of the inverters and converters are maintained and the system is set to receive a command from the master controller. When the command is given, the drive system begins to operate and the dc-link voltages are regulated to the nominal voltage of 680 V. Therefore, the motor accelerates the

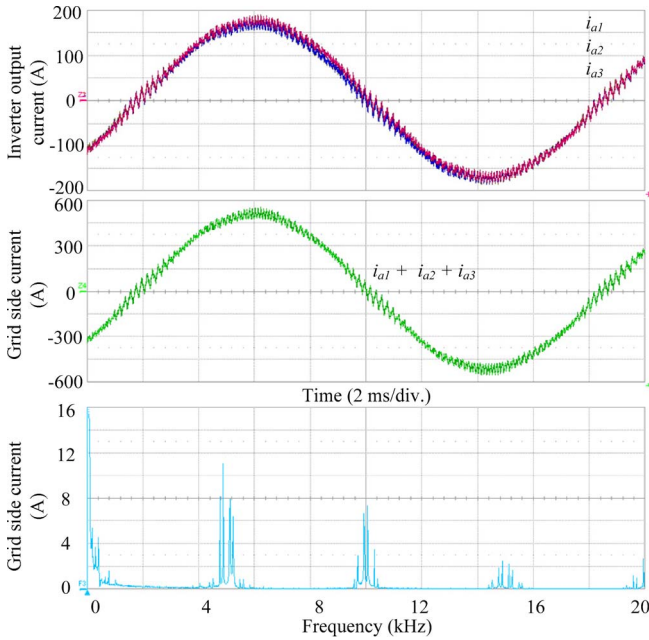


Fig. 15. Grid-side current waveform without PWM interleaving.

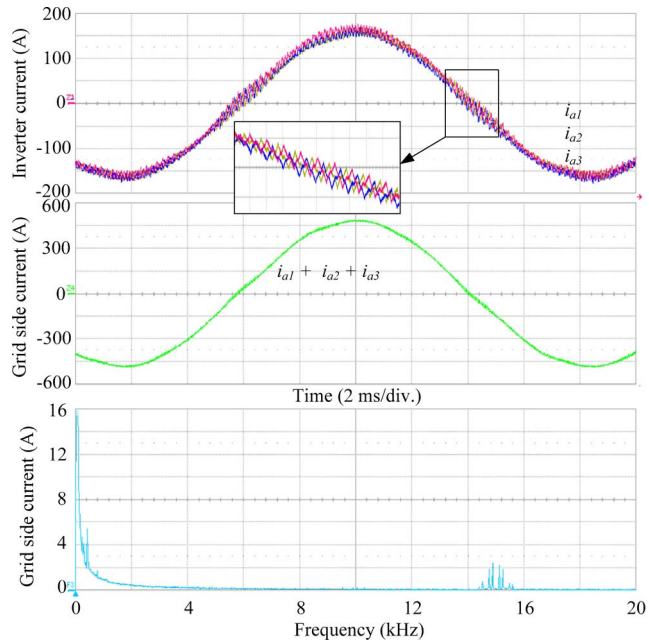


Fig. 16. Grid-side current waveform with PWM interleaving.

main sheave up to the maximum speed according to the speed reference profile. The acceleration waveform indicates the measured acceleration data at the car. As the speed increases, the car acceleration rate is kept constant. The load torque, however, is not constant because it is determined by the mechanical loss, the wind resistance, and the weight imbalance in the test tower. In this experiment, the constant speed section was very short owing to the short stroke.

To improve the quality of the grid-side current, PWM interleaving was applied. The effect of this is shown in Figs. 15 and 16. The converter output currents and the grid-side current without the PWM interleaving technique are represented in Fig. 15. The converter output currents of each set are nearly identical. Thus, the grid-side current, which is the sum of the converter

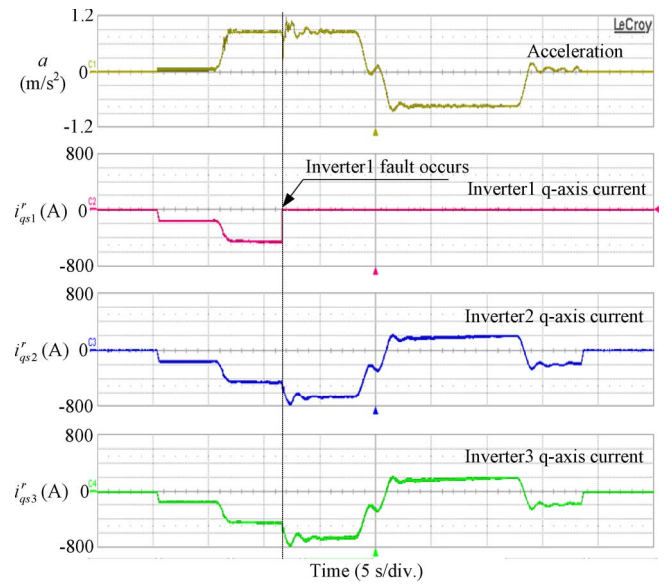


Fig. 17. Operation of the elevator in the test tower during an Inverter 1 fault.

output currents, also has considerable switching current ripple. The magnitude values of the current near the switching, second-order, and third-order frequencies are approximately 10, 7.5, and 2 A, respectively. The experimental results under the same operating condition but with PWM interleaving are shown in Fig. 16. The current ripple of each phase is shifted from the next one by one-third of the switching period and is thus canceled out. As a result, the magnitude values of the ripple current near the switching frequency and at twice the switching frequency are dramatically reduced.

To determine the system fault tolerance, an inverter fault was forced to occur during the acceleration of the car in the test tower. The inverter fault-tolerant operation is shown in Fig. 17. When the fault occurs, all of the Inverter 1 gating is turned off. While the Inverter 1 current is reduced to zero, the outputs of the other two inverters are increased to support the portion of the faulty inverter. That is, before the fault, each inverter delivers one-third of the motor power, but after the fault, each nonfaulty inverter delivers one half of the motor power. During this transient, the acceleration flutters because the fault acts as an impulse shock, which is transferred to the car by the ropes. Sensitive passengers may feel this small variation of the acceleration but will not likely consider this as a fault because it is short and neither continuous nor repeated.

V. CONCLUSION

The advent of modern high-rise buildings has brought about the need for high-speed elevator systems. The conventional three-phase electric drive system for high-speed elevators cannot suitably satisfy the specifications of such a new ultrahigh-speed elevator. This paper has concentrated on development of a nine-phase PMSM and its drive system for an ultrahigh-speed elevator. A mathematical model of the nine-phase PMSM was evaluated and simplified by the symmetry of winding sets and current controllers. Using the simplified mathematical model, the nine-phase PMSM could be controlled by a conventional three-phase current control algorithm. The validity of the

simplified model and the control system of the nine-phase motor was verified by the experimental results.

The experimental results obtained during the operation of an elevator from the first to the 47th floor in an elevator test tower were presented to validate the feasibility of the developed drive system. Fault-tolerant operation was also tested to assess the improvement of the system reliability. It was concluded that the developed system and its controller are effective and reliable in ensuring the desired operation of the elevator.

REFERENCES

- [1] J. Ho, "Elevator/escalator trends in Southeast Asia," *Hitachi Rev.*, vol. 42, no. 5, pp. 179–184, Oct. 1993.
- [2] D. W. Chung, H. M. Ryu, Y. M. Lee, L. W. Kang, S. K. Sul, S. J. Kang, J. H. Song, J. S. Yoon, K. H. Lee, and J. H. Suh, "Drive systems for high-speed gearless elevators," *IEEE Ind. Appl. Mag.*, vol. 7, no. 5, pp. 52–56, Sep./Oct. 2001.
- [3] M. A. Abbas, R. Christen, and T. M. Jahns, "Six-phase voltage source inverter driven induction motor," *IEEE Trans. Ind. Appl.*, vol. IA-20, no. 5, pp. 1251–1259, Sep./Oct. 1984.
- [4] R. Kianinezhad, B. Nahid-Mobarakkeh, L. Baghli, F. Betin, and G. A. Capolino, "Modeling and control of six-phase symmetrical induction motor under fault condition due to open phases," *IEEE Trans. Ind. Electron.*, vol. 55, no. 5, pp. 1966–1977, May 2008.
- [5] M. A. Shamsi-Nejad, B. Nahid-Mobarakkeh, S. Pierfederici, and F. Meibody-Tabar, "Fault tolerant and minimum loss control of double-star synchronous motors under open phase conditions," *IEEE Trans. Ind. Electron.*, vol. 55, no. 5, pp. 1956–1965, May 2008.
- [6] E. Levi, "Multiphase electric machines for variable-speed applications," *IEEE Trans. Ind. Electron.*, vol. 55, no. 5, pp. 1893–1909, May 2008.
- [7] N. Toshiaki, K. Hideya, S. Youichi, and N. Shigeo, "World's fastest elevator (1,010 m/min)," *Toshiba Rev.*, vol. 57, no. 6, pp. 58–63, 2002.
- [8] R. H. Nelson and P. C. Krause, "Induction machine analysis for arbitrary displacement between multiple winding sets," *IEEE Trans. Power App. Syst.*, vol. PAS-93, no. 3, pp. 841–848, May/Jun. 1974.
- [9] E. A. Klingshirn, "High phase order induction motors, Part I—Description and theoretical considerations," *IEEE Trans. Power App. Syst.*, vol. PAS-102, no. 1, pp. 47–53, Jan. 1983.
- [10] E. A. Klingshirn, "High phase order induction motors: Part II—Experimental results," *IEEE Trans. Power App. Syst.*, vol. PAS-102, no. 1, pp. 54–59, Jan. 1983.
- [11] A. A. Rockhill and T. A. Lipo, "A simplified model of a nine phase synchronous machine using vector space decomposition," in *Conf. Rec. IEEE PEMWA*, 2009, pp. 1–5.
- [12] Y. Zhao and T. A. Lipo, "Space vector PWM control of dual three-phase induction machine using vector space decomposition," *IEEE Trans. Ind. Appl.*, vol. 31, no. 5, pp. 1100–1109, Sep./Oct. 1995.
- [13] R. Bojoi, F. Farina, F. Profumo, and A. Tenconi, "Dual-three phase induction machine drives control—A survey," *IEEE Trans. Ind. Appl.*, vol. 126, no. 4, pp. 420–429, 2006.
- [14] R. Bojoi, F. Farina, M. Lazzari, F. Profumo, and A. Tenconi, "Analysis of the asymmetrical operation of dual three-phase induction machines," in *Conf. Rec. IEEE IEMDC*, Jun. 2003, pp. 429–435.
- [15] L. De Camillis, M. Matuonto, A. Monti, and A. Vignati, "Optimizing current control performance in double winding asynchronous motors in large power inverter drives," *IEEE Trans. Power Electron.*, vol. 16, no. 5, pp. 676–685, Sep. 2001.
- [16] R. Bojoi, A. Tenconi, F. Profumo, G. Griva, and D. Martinello, "Complete analysis and comparative study of digital modulation techniques for dual three-phase AC motor drives," in *Conf. Rec. IEEE PESC*, 2002, pp. 851–857.
- [17] R. Bojoi, M. Lazzari, F. Profumo, and A. Tenconi, "Digital field-oriented control for dual three-phase induction motor drives," *IEEE Trans. Ind. Appl.*, vol. 39, no. 3, pp. 752–760, May/Jun. 2003.
- [18] F. B. del Blanco, M. W. Degner, and R. D. Lorenz, "Dynamic analysis of current regulators for AC motors using complex vectors," *IEEE Trans. Ind. Appl.*, vol. 35, no. 6, pp. 1424–1432, Nov./Dec. 1999.
- [19] D. W. Novotny and T. A. Lipo, *Vector Control and Dynamics of AC Drives*. Oxford, U.K.: Clarendon, 1996.
- [20] D. W. Chung, J. S. Kim, and S. K. Sul, "Unified voltage modulation technique for real time three-phase power conversion," *IEEE Trans. Ind. Appl.*, vol. 34, no. 2, pp. 374–380, Mar./Apr. 1998.



Eunsoo Jung (S'08) received the B.S. degree in mechanical and aerospace engineering from Seoul National University, Seoul, Korea, in 2005, where he is currently working toward the Ph.D. degree in electrical engineering and computer science.

His current research interests include electric machine drives and power-converter circuits.



Hyunjae Yoo (S'05–M'10) received the B.S. degree in electronic and electrical engineering from Kyungpook National University, Daegu, Korea, in 2003, and the M.S. and Ph.D. degrees in electrical engineering and computer science from Seoul National University, Seoul, Korea, in 2005 and 2009, respectively.

Since 2009, he has been with Samsung Heavy Industries Company, Ltd., Seoul. His current research interests are high-power power converter control for wind turbines, medium-voltage power converter drives,

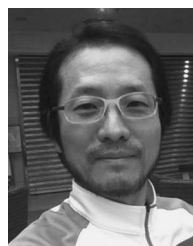
and power control algorithms for renewable energy.



Seung-Ki Sul (S'78–M'80–SM'98–F'00) was born in Korea in 1958. He received the B.S., M.S., and Ph.D. degrees in electrical engineering from Seoul National University, Seoul, Korea, in 1980, 1983, and 1986, respectively.

From 1986 to 1988, he was an Associate Researcher with the Department of Electrical and Computer Engineering, University of Wisconsin, Madison. From 1988 to 1990, he was a Principal Research Engineer with Gold-Star Industrial Systems Company. Since 1991, he has been a Professor with

the School of Electrical Engineering and Computer Science, Seoul National University, where, from 2005 to 2007, he was the Vice Dean and, from 2008 to 2011, was the President of the Korea Electrical Engineering and Science Research Institute. His current research interests are power-electronic control of electric machines, electric/hybrid vehicle drives, and power-converter circuits.



Hong-Soon Choi was born in Korea in 1963. He received the B.S., M.S., and Ph.D. degrees in electrical engineering from Seoul National University, Seoul, Korea, in 1986, 1988, and 2000, respectively.

From 1988 to 1994, he was a Senior Research Engineer with Samsung Electro-Mechanics Company. From 1995 to 1997, he was a Senior Researcher with the Korea Electrical Engineering and Science Research Institute. From 1997 to 2003, he was a Co-Founder and a Research Director with KOMOTEK Company, Sungnam, Korea, which develops and produces precision motors.

From 2003 to 2006, he was a Research Professor with Sungkyunkwan University, Seoul. Since 2007, he has been a Professor in the School of Electrical Engineering, Kyungpook National University, Daegu, Korea. His current research interests are design of electric machines, and multiphysics of electrics and mechanics.



Yun-Young Choi was born in Korea in 1974. He received the B.S. and M.S. degrees in electrical engineering from Kangwon National University, Chuncheon, Korea, in 1999 and 2001, respectively.

Since 2001, he has been working for the Technical R&D Center, Hyundai Elevator Company, Ltd., Icheon, Korea, as a Research Engineer. His current research interests are high-performance alternating-current motor drives and high-speed elevator systems.